Elementary response triggered by transducin in retinal rods

Wendy W. S. Yue[a,b,c,1,2], Daniel Silverman[a,b,c,1], Xiaozhi Ren[a,b,3], Rikard Frederiksen[d,4], Kazumi Sakai[e], Takahiro Yamashita[e], Yoshinori Shichida[e,f], M. Carter Cornwall[d], Jeannie Chen[g,h], and King-Wai Yau[a,b,i,5]

[a]Solomon H. Snyder Department of Neuroscience, Johns Hopkins University School of Medicine, Baltimore, MD 21205; [b]Center for Sensory Biology, Johns Hopkins University School of Medicine, Baltimore, MD 21205; [c]Biochemistry, Cellular and Molecular Biology Graduate Program, Johns Hopkins University School of Medicine, Baltimore, MD 21205; [d]Department of Physiology and Biophysics, Boston University School of Medicine, Boston, MA 02118; [e]Department of Biophysics, Kyoto University, Kyoto 606-8502, Japan; [f]Research Organization for Science and Technology, Ritsumeikan University, Kusatsu, Shiga 525-8577, Japan; [g]Zilkha Neurogenetic Institute, Keck School of Medicine, University of Southern California, Los Angeles, CA 90089; [h]Department of Physiology and Biophysics, Keck School of Medicine, University of Southern California, Los Angeles, CA 90089; and [i]Department of Ophthalmology, Johns Hopkins University School of Medicine, Baltimore, MD 21205

Contributed by King-Wai Yau, January 16, 2019 (sent for review October 17, 2018; reviewed by Petri Ala-Laurila and Theodore G. Wensel)

G protein-coupled receptor (GPCR) signaling is crucial for many physiological processes. A signature of such pathways is high amplification, a concept originating from retinal rod phototransduction, whereby one photoactivated rhodopsin molecule (Rho*) was long reported to activate several hundred transducins (G_T*s), each then activating a cGMP-phosphodiesterase catalytic subunit (G_T*·PDE*). This high gain at the Rho*-to-G_T* step has been challenged more recently, but estimates remain dispersed and rely on some nonintact rod measurements. With two independent approaches, one with an extremely inefficient mutant rhodopsin and the other with WT bleached rhodopsin, which has exceedingly weak constitutive activity in darkness, we obtained an estimate for the electrical effect from a single G_T*·PDE* molecular complex in intact mouse rods. Comparing the single-G_T*·PDE* effect to the WT single-photon response, both in *Gcaps*$^{-/-}$ background, gives an effective gain of only ∼12–14 G_T*·PDE*s produced per Rho*. Our findings have finally dispelled the entrenched concept of very high gain at the receptor-to-G protein/effector step in GPCR systems.

G protein-coupled receptor | rhodopsin | apo-opsin | rod phototransduction | signal amplification

G protein-coupled receptors (GPCRs) function in diverse cellular signaling pathways such as sensory transduction, synaptic transmission, hormone signaling, and inflammatory responses. In recent decades, there has been an ever-expanding identification of GPCRs and their downstream signaling components in various cell types. Furthermore, advances in structural biology and biochemistry have elucidated the different conformational states of GPCRs and the downstream components' molecular interacting domains. Nonetheless, much less is known about the dynamics of these component interactions, especially in the native cellular environment.

Rod phototransduction, in many ways, has been a particularly useful model of GPCR signaling. Apart from being one of the very first GPCR pathways discovered, the high photosensitivity of rods permits their light response to be resolved and analyzed down to the level of action of a single photoactivated rhodopsin molecule (Rho*; i.e., single-photon response) (1), providing an important basis for understanding phototransduction and signal processing through the retinal circuitry. Rho* activates the G protein transducin (G_T), which in turn activates a cGMP-phosphodiesterase (PDE) to hydrolyze cGMP, lowering the latter's concentration and closing some cyclic–nucleotide-gated (CNG), nonselective cation channels that are open in darkness. Early work suggested that many hundreds of active G_T molecules (G_T*s) are generated by a single Rho* (2), with each G_T* (consisting of its α-subunit, G_Tα, with GTP bound) then activating a PDE molecular complex (3) (represented by G_T*·PDE*; *Discussion*). A large G_T*/Rho* ratio therefore offered seemingly an attractive amplification mechanism for producing the high photosensitivity of rods (2). For more than 30 y, this concept of high gain from rhodopsin to G protein has taken hold as a textbook dogma (4–6), to such an extent as to become also a general signature of GPCR signaling (4, 7, 8). Within the field of phototransduction, this gain is more recently suggested (9) to be much lower than originally proposed, but not with unanimous agreement. Above all, recent estimates still depend partly on nonintact rod measurements and/or computational modeling (*SI Appendix*, *Supplementary Text I*). As such, the concept of low gain at the receptor-to-G protein step has not penetrated widely outside of the field. At the same time, the originally proposed large amplification has discouraged further dissection of the single-photon response into its constituent single-G_T*·PDE* effects for a more thorough understanding of the visual process.

In this work, we present measurements of the single-G_T*·PDE* effect in live, intact rods by two independent methods that exploit specific situations conferring weak signaling from Rho* to G_T*. First, a targeted mutation of rhodopsin's G

Significance

For decades, amplification at the step of rhodopsin–G protein (transducin) interaction in rod phototransduction has been believed to be ∼500, a high value often generalized to other G protein-coupled receptor pathways. Recently, there have been indications that this amplification may be considerably lower. Nonetheless, disputes persist because of the large variation in estimates obtained by different groups, plus the drawback that some key measurements used in such estimates came from experiments on nonintact rods. As such, the dogma continues in textbooks. Here, we report experiments entirely on intact rods to measure the effect of a single transducin molecule via the transducin–phosphodiesterase (PDE) complex, and conclude that a photoexcited rhodopsin activates effectively only ∼12–14 transducin–PDE effector complexes.

Author contributions: W.W.S.Y., D.S., J.C., and K.-W.Y. designed research; W.W.S.Y., D.S., X.R., R.F., K.S., T.Y., Y.S., M.C.C., and J.C. performed research; W.W.S.Y., D.S., X.R., R.F., K.S., T.Y., Y.S., M.C.C., and J.C. analyzed data; and W.W.S.Y., D.S., and K.-W.Y. wrote the paper.

Reviewers: P.A.-L., University of Helsinki; and T.G.W., Baylor College of Medicine.

The authors declare no conflict of interest.

[1]W.W.S.Y. and D.S. contributed equally to this work.

[2]Present address: Department of Physiology, University of California, San Francisco, CA 94158.

[3]Present address: Cell Line Development Skill Center, Sanofi Global Biopharmaceutics Development, Framingham, MA 01701.

[4]Present address: Jules Stein Eye Institute, University of California, Los Angeles, CA 90095.

[5]To whom correspondence should be addressed. Email: kwyau@jhmi.edu.

This article contains supporting information online at www.pnas.org/lookup/suppl/doi:10.1073/pnas.1817781116/-/DCSupplemental.

Published online February 22, 2019.

protein-binding site (REY-Rho) (10, 11) allowed us to extract a light-evoked single-G_T*·PDE* effect in native mouse rods. Second, we took advantage of the weak constitutive activity (12) of WT apo-opsin (WT-Opn; i.e., photobleached Rho, which lacks chromophore) to quantify the randomly-triggered single-G_T*·PDE* effects occurring in darkness. Among a number of observations, we most importantly found that the WT single-photon response is probably composed of only 12–14 G_T*·PDE*s, contrary to the long-held belief of a much larger number. We provide a rationalization for this revised picture of GPCR signaling.

Results

Mutation at Rho's Glu-Arg-Tyr Motif Severely Reduces G_T Activation in Mouse Rods Without Affecting Downstream Phototransduction Cascade. Our first strategy for measuring the single-G_T*·PDE* effect in intact rods was to reduce drastically the affinity of Rho* for G_T so that a Rho* would activate at most one G_T* in its active lifetime, i.e., being unproductive in most cases, and only occasionally leading to a single G_T* according to the Poisson distribution. As such, the single-G_T*·PDE* effect would become the elementary unit underlying the light response, extractable by fluctuation analysis.

Previous heterologous-expression studies have shown that mutating Rho's G protein-interaction motif from Glu-Arg-Tyr (i.e., ERY) to REY severely impaired its binding to G_T without affecting light absorption (10, 11). Thus, we made such a mouse line (denoted $Rho^{REY/REY}$) and bred it into $Gcaps^{-/-}$ background. The $Gcaps^{-/-}$ genotype removed in rods the expression of the guanylate cyclase-activating proteins (13) GCAP1 and GCAP2, which normally regulate cGMP synthesis via Ca^{2+} feedback to produce light adaptation in phototransduction. The single-photon response of $Gcaps^{-/-}$ rods is approximately fivefold as large as normal (13) and therefore facilitates our data analysis of small signals. Henceforth, $Rho^{WT/WT}$;$Gcaps^{-/-}$ and $Rho^{REY/REY}$;$Gcaps^{-/-}$ lines are referred to as *WT* and *REY*, respectively, when appropriate.

The *REY* retina shows normal morphology (Fig. 1*A*). Moreover, REY-Rho targets correctly to rod outer segments (Fig. 1*B*) and has normal light absorption in vitro (Fig. 1*C*) as well as in situ (Fig. 1*D*), with peak absorption at 500 nm. Microspectrophotometry suggested an expression of REY-Rho slightly lower than *WT* (note peak amplitudes in Fig. 1*D*), but this does not affect data analysis and conclusions. The levels of various rod-phototransduction proteins, including $G_T\alpha$, are also normal in *REY* retinae (Fig. 1*E*).

REY rods had similar dark-current amplitudes but slower response kinetics than *WT* (Fig. 2*A* and *SI Appendix*, Table S1A). To examine whether the slower kinetics came from the mutant pigment or from secondary changes downstream, we expressed WT human red cone pigment transgenically at a low level in *REY* rods (i.e., $hOpn1lw^{Tg}$;$Rho^{REY/REY}$;$Gcaps^{-/-}$). Previously, we found that transgenic human red cone pigment produced responses with normal Rho-like kinetics in *WT* rods (14), thus serving here as a useful test case. By using 560-nm light that preferentially activates the red cone pigment over REY-Rho, we found that $hOpn1lw^{Tg}$;$Rho^{REY/REY}$;$Gcaps^{-/-}$ rods gave small responses with normal kinetics, as opposed to the slowed responses of *REY* rods (Fig. 2*B*, *Inset*). Thus, the REY mutation does not affect signal transduction downstream.

More importantly, as a proxy for light sensitivity, the flash intensity required to produce a half-maximal response (ρ) in *WT* and *REY* rods was found to be, respectively, ~6 and ~46,168 photons·μm^{-2} at 500 nm, differing by >7,400-fold (Fig. 2*C*; see also flash sensitivities in *SI Appendix*, Table S1A). Given the normal light absorption by REY-Rho, as well as its near-normal expression level and those of other phototransduction components, this drastically lower sensitivity is consistent with REY-Rho*'s exceedingly low efficiency in activating G_T.

In short, the REY mutation greatly reduced the functional coupling between Rho* and G_T, potentially providing a tool for estimating the single-G_T*·PDE* effect.

Unitary Response of *REY* Rods Represents Single-G_T*·PDE* Effect. We carried out fluctuation analysis to extract the elementary unit underlying the light responses of *WT* and *REY* rods, respectively.

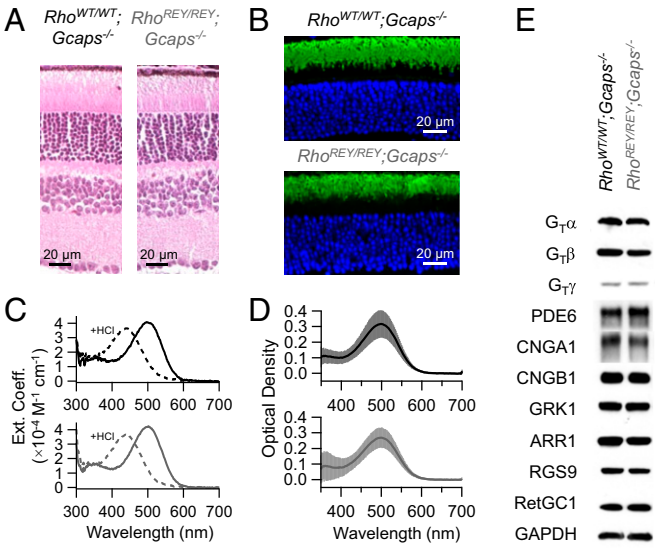

Fig. 1. Characterization of $Rho^{REY/REY}$;$Gcaps^{-/-}$ retinae and heterologously expressed REY-Rho. (*A*) Paraffin sections of 2-mo-old *WT* (*Left*) and *REY* (*Right*) retinae stained by H&E. (*B*) Paraffin sections of 2-mo-old *WT* (*Top*) and *REY* (*Bottom*) retinae immunostained for rhodopsin. DAPI marks the outer nuclear layer. (*C*) Extinction coefficients of WT-Rho (solid black trace) and REY-Rho (solid gray trace) measured by in vitro spectrophotometry. Acid denaturation (dashed traces; *SI Appendix, Supplementary Methods*) confirmed that both pigments were present at the same amount. Two other experiments gave similar measurements for REY-Rho. (*D*) Absorption spectra of *WT* (*Top*) and *REY* (*Bottom*) rods measured by in situ microspectrophotometry (*SI Appendix, Supplementary Methods*; mean ± SD; n = 8). (*E*) Western blots showing the expression levels of various phototransduction components in extracts of *WT* (*Left*) and *REY* (*Right*) retinae. ARR1, arrestin isoform 1; CNGA1 and CNGB1, A1 and B1 subunit of the rod CNG channel, respectively; GRK1, G protein receptor kinase isoform 1; $G_T\alpha$, $G_T\beta$, and $G_T\gamma$, α, β, and γ subunit of G_T, respectively; PDE6, rod phosphodiesterase isoform 6; RetGC1, retinal guanylate cyclase isoform 1; RGS9, regulator of G protein signaling isoform 9. GAPDH was used as control for protein concentration in total extracts.

Rods were challenged with a series of repeated, identical diffuse flashes to elicit an ensemble of small responses (Fig. 3*A*, *Top*) within the linear foot of the respective intensity-response relations (Fig. 2*C*). In *WT* rods, each Rho* produces many G_T*·PDE*s. In *REY* rods, however, REY-Rho*'s exceedingly low signaling efficiency (Fig. 2*C*) means that it triggers mostly nothing—sometimes only a single-G_T*·PDE* effect—and almost never more than a single-G_T*·PDE* effect, making the single-G_T*·PDE* effect the unitary response. For both genotypes, we quantified the response fluctuations by measuring the ensemble mean (μ) and ensemble variance (σ^2) of the flash responses (Fig. 3*A*, *Left* and *Right*). Whether *WT* or *REY* rods, the response variance and the square of the mean response matched fairly well in waveform for most cells examined, consistent with the stochastic occurrence of fairly constant unitary events. From the Poisson distribution, we obtained the unitary amplitude, a, from $a = \sigma^2/\mu$ at the response's initial rising phase (*SI Appendix, Supplementary Methods*), yielding 3.11 ± 0.43 pA for *WT* rods (mean ± SD, n = 15 rods; black symbols in Fig. 3*B*, *Left*; cf. refs. 13 and 15) and 0.13 ± 0.04 pA for *REY* rods (n = 12 rods; gray symbols in Fig. 3*B*, *Right*).

To verify that *REY* rods' unitary responses indeed reflected the effect of just a single G_T*·PDE*, we shortened REY-Rho*'s lifetime by using a transgenic line ($Grk1^{S561L}$) that has a higher than normal expression of rhodopsin kinase, GRK1 (16, 17), thus speeding up the phosphorylation of REY-Rho* and hence its shutoff. As such, if the unitary response by normal-life REY-Rho* involved more than one G_T*, a shorter-life REY-Rho* might lead to fewer G_T*s on average, and thereby a smaller

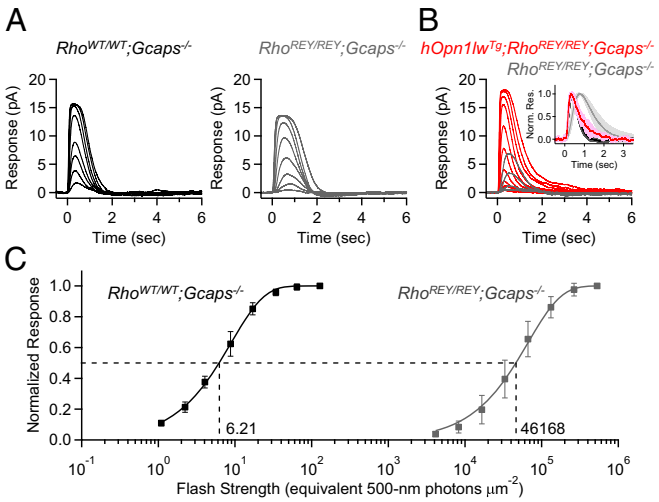

Fig. 2. Photoresponses of *REY* rods. (*A*) Response families of a *WT* rod (*Left*) and a *REY* rod (*Right*), both in *Gcaps*$^{-/-}$ background. *WT* was exposed to 500-nm light; *REY* to white light because of its weak sensitivity. Averaged responses to 10-ms flashes at time 0 are shown. (*B*) Superimposed responses of a *hOpn1lw*^{Tg};*Rho*$^{REY/REY}$;*Gcaps*$^{-/-}$ rod (red) and a *REY* rod (gray) to flashes of the same set of intensities at 560 nm (λ_{max} of transgenic red cone pigment). Averaged responses to 30-ms flashes at time 0 are shown. (*Inset*) Small averaged responses (mean ± SD) of *hOpn1lw*^{Tg};*Rho*$^{REY/REY}$;*Gcaps*$^{-/-}$ (red, $n = 6$), *WT* (black, $n = 15$), and *REY* (gray, $n = 11$) rods, overlaid and normalized at peak for kinetics comparisons. Absolute amplitudes are 0.95 pA, 1.93 pA, and 1.58 pA, respectively. (*C*) Intensity–response relations of *WT* (black, $n = 8$) and *REY* (gray, $n = 16$) rods. Fitting with a single saturating-exponential function gave half-saturating flash strengths (ρ) of 6.21 and 46,168 (equivalent 500-nm) photons·μm^{-2} for *WT* and *REY* rods, respectively. Data points are means ± SD.

mutant single-photon response. In contrast, if the *REY* rod's single-photon response involved literally no more than one G_T*, a shorter REY-Rho* lifetime in the *Grk1*^{S561L} genotype should not affect the unitary size but only reduce REY-Rho*'s probability of producing any G_T*, thus lowering sensitivity further (see flash sensitivities in *SI Appendix*, Table S1A). Indeed, although the *Grk1*^{S561L} background reduced the control WT-Rho*'s single-photon response to ∼1.3 pA (red symbols in Fig. 3*B*, *Left*; cf. ref. 17), it left REY-Rho*'s unitary-response amplitude unchanged (pink symbols in Fig. 3*B*, *Right*). Conversely, reducing GRK1's level with the *Grk1*$^{+/-}$ background (18) increased WT-Rho*'s single-photon response (green symbols in Fig. 3*B*, *Left*; cf. ref. 17), but again did not affect REY-Rho*'s unitary response (dark green symbols in Fig. 3*B*, *Right*), suggesting that the deficiency in G_T activation by REY-Rho is so severe that it cannot be overcome easily by a longer REY-Rho* lifetime. Note that the GRK mutations did affect the kinetics of the light response from REY-Rho (Fig. 3*B*, *Right*, *Top*; see also *SI Appendix*, Fig. S1), confirming an effect on the REY-Rho* lifetime. In fact, the *Grk1*^{S561L} transgene had an obviously greater impact on the kinetics of small responses in the *REY* background than in *WT* rods (Fig. 3*B* and *SI Appendix*, Table S1A), which may suggest that the inactivation of REY-Rho* has become the rate-limiting step in photoresponse termination in these rods.

As an alternative to manipulating REY-Rho*'s lifetime for validating the single-G_T*·PDE* effect, we lowered drastically the expression level of G_T so as to reduce the encounters between Rho* and G_T. With the same reasoning described here earlier, we expected this manipulation to reduce the unitary response of *WT* but not *REY* rods. To this end, we generated a mouse line (*Gnat1*^{Tg};*Gnat1*$^{-/-}$;*Rho*$^{WT/WT}$;*Gcaps*$^{-/-}$) with rod $G_T\alpha$ expressed transgenically under the mouse opsin promoter (Fig. 4*A*) and the endogenous rod $G_T\alpha$ gene ablated (19). This genotype brought rod $G_T\alpha$ level down to ∼6% of *WT* (Fig. 4*B*), leading to an approximately fourfold decrease in light sensitivity (Fig. 4*C*), but did not affect light absorption by pigment or protein expression of phototransduction components in *WT* and *REY* backgrounds (Fig. 4 *D* and *E*).

Underexpression of $G_T\alpha$ decreased the unitary response amplitude in *WT* rods by two to three fold (blue symbols in Fig. 3*C*, *Left*), which is quite a small change given the large decrease in $G_T\alpha$ protein level (∼17-fold). This observation may be explained by a much higher encounter rate between Rho* and G_T normally in rods (estimated to be ∼17,000 s^{-1} for mammalian rods at 37 °C; see ref. 20) compared with the rate of G_T* production per Rho*, presumably reflecting the time required for G_T activation (i.e., GDP/GTP exchange in $G_T\alpha$ and the subsequent dissociation of G_T* from Rho*) during which any further collisions between Rho* and other G_Ts would be inconsequential. Thus, although the Rho*-G_T encounter rate may be diffusion-limited and roughly proportional to G_T concentration (20), this rate can be much lower without a large effect on the single-photon–response amplitude. Incidentally, apart from its smaller amplitude, the single-photon response of *Gnat1*^{Tg};*Gnat1*$^{-/-}$;*Rho*$^{WT/WT}$;*Gcaps*$^{-/-}$ rods also had a recovery time constant, τ_{rec}, approximately two times that in *WT* rods (Fig. 3*C* and *SI Appendix*, Table S1A; see legends), possibly suggesting that $G_T\alpha$ may shut off more slowly when underexpressed.

More importantly, the unitary-response amplitude remained constant in *REY* rods underexpressing $G_T\alpha$ (light blue symbols in Fig. 3*C*, *Right*), further supporting the notion that each REY-Rho* activated G_T with exceedingly low probability, thereby producing literally at most one G_T*·PDE*. Taken altogether, we have succeeded in isolating and estimating the response triggered by a single G_T*·PDE*.

WT-Opn Produces Detectable Electrical Noise After a Bleach. To evaluate the single-G_T*·PDE* effect with an alternative method that does not involve mutating Rho, we quantified the constitutive activity of WT-Opn in darkness (i.e., Rho without chromophore). Cornwall and Fain (12) first established Opn's constitutive activity, reporting each Opn molecule in salamander to be ∼10^{-7}-fold as effective in activating transduction as a steady light producing ∼1 Rho* s^{-1}, i.e., exceedingly weak in activity (see also ref. 21). A similar observation was made in mouse rods (22). We interpret this huge quantitative difference in activity between Rho* and Opn to reflect one or both of two factors: (*i*) the very low probability of Opn being active (formally represented by its only occasional transitioning into an active state, Opn*, i.e., Opn $\rightleftharpoons$ Opn*) and (*ii*) a very low probability of Opn* successfully producing any G_T*, e.g., as a result of Opn*'s short dwell time or Opn*'s weak efficacy in activating G_T. Our rationale, nonetheless, is that, no matter how unlikely to occur, the unitary event underlying this activity should still involve no less than a single-G_T*·PDE* effect and is therefore resolvable based on our findings with mutant-Rho described earlier.

Fig. 5*A* shows a continuous recording in darkness from a *WT* rod (in *Gcaps*$^{-/-}$ background) subjected to an intense flash at time 0 that saturated the response and produced an ∼1% bleach of the cell's rhodopsin (*Methods* and *SI Appendix*, *Supplementary Methods*). Before bleaching, the dark current was relatively quiet except for some level of "continuous" noise (23, 24) and occasional blips ("discrete" events) representing spontaneous (i.e., thermal) isomerization of single Rho molecules (23, 25). After bleaching, the slowly recovering dark current became much noisier for minutes, reflecting sustained Rho* activity (26, 27). Also, this increase in noise arose partly from constitutive Opn activity. To focus on Opn-associated noise, we kept the rods in darkness for 1–3 h after a bleach to allow a near-complete decay of Rho* to Opn (22) before proceeding to recordings (*Methods*). Normally, Opn in situ would not persist indefinitely because of its reconversion to Rho by free chromophore from the retinal pigment epithelium (RPE); in our preparation, however, this regeneration did not occur because the RPE was removed (*Methods*). It was literally impossible to record for multiple hours from the same cell before and after bleaching, so we compared averaged data from cohorts of unbleached and bleached cells.

Fig. 5*B* shows sample dark recordings from *WT* rods, either unbleached (Fig. 5*B*, *Left*) or at different times after a 5% bleach

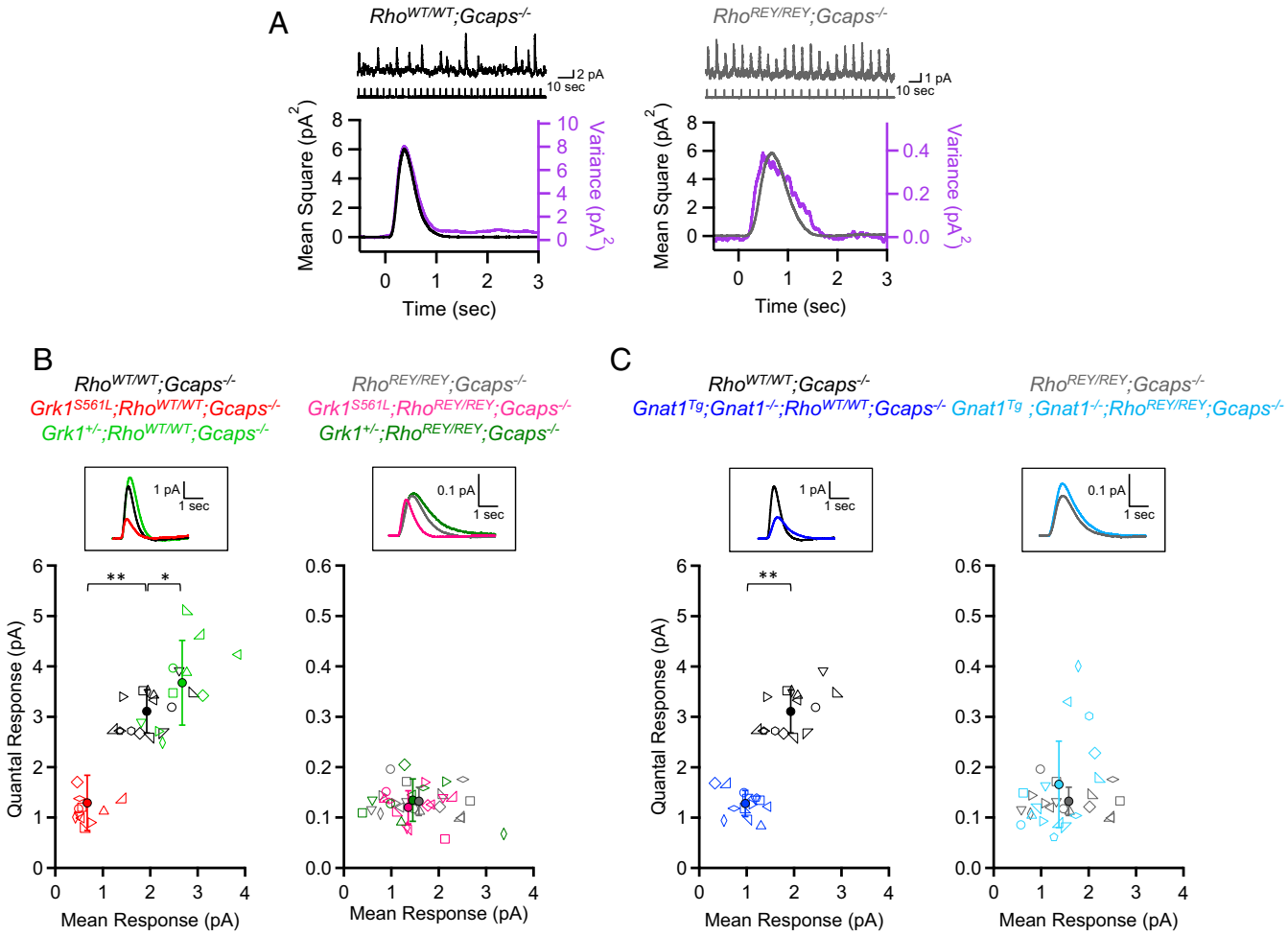

Fig. 3. Estimate of single-G_T*·PDE* effect from REY-Rho* responses. (*A*, *Top*) Responses of a *WT* rod (*Left*) and a *REY* rod (*Right*) to repetitive 10-ms, 500-nm flashes (vertical bars). For *REY* rods, multiple single-G*·PDE* effects were elicited at the chosen intensity, and therefore the probability of observing failures was low. (*A*, *Bottom*) Square of the ensemble mean (black on left; gray on right) overlaid on the ensemble variance (purple) of the responses. The cells are the same as at *Top*. Ratio between ensemble variance and ensemble mean allows estimation of the unitary response amplitude (*Methods* and *SI Appendix, Supplementary Methods*). (*B*, *Bottom*) Peak amplitudes of unitary responses of rods with WT (*Left*) or REY (*Right*) rhodopsin plotted against the mean response peak. The $Grk1^{S561L}$ (red on left; pink on right) and $Grk1^{+/-}$ (light green on left; dark green on right) mutations were used to shorten and lengthen Rho* lifetime, respectively (see text). Each open symbol represents one cell, with identical symbols representing the same cell being stimulated at multiple intensities. Solid circles are means ± SD. Brackets denote pairwise Student's *t* tests on quantal response amplitudes with $0.0001 \leq P < 0.05$ and $P < 0.0001$ marked by single and double asterisks, respectively. No statistically significant differences between genotypes on right ($P = 0.35$ between $Grk1^{S561L}$;$Rho^{REY/REY}$;$Gcaps^{-/-}$ and *REY*; $P = 0.91$ between $Grk1^{+/-}$;$Rho^{REY/REY}$;$Gcaps^{-/-}$ and *REY*). (*B*, *Top*) Averaged single-photon–response profiles of rods of the corresponding genotypes (see *SI Appendix*, Table S1 for kinetics measurements). (*C*) Similar to *B* but with genetic manipulation on $G_T\alpha$. The genotype $Gnat1^{Tg}$;$Gnat1^{-/-}$ reduces $G_T\alpha$ expression to ~6% of *WT* (Fig. 4). The difference between genotypes on right is not statistically significant ($P = 0.20$).

(Fig. 5*B*, *Right*), indicating the elevated dark noise long after bleaching. We confirmed that the postbleach noise arose from constitutive activation of G_T by Opn* because it quieted down upon converting Opn to Rho with exogenous 11-*cis*-retinal (Fig. 5*B*, *Right*, *Bottom*). The aggregate presence of Opn led to random unitary Opn* effects that summated to produce a postbleach shift (slight decrease) in the mean dark current and an increase in the dark-current variance. In the collected data of Fig. 5*C*, *Top* and *Bottom*, the horizontal blue lines indicate cohort-averaged mean and noise variance of post–5%-bleach dark current against time vs. cohort-averaged control dark values (Fig. 5*C*, black lines), both excluding visible discrete events (marked by stars in Fig. 5*B*; see *SI Appendix*, *Supplementary Methods*). These postbleach parameters returned nearly to unbleached levels upon regeneration of Opn to Rho by exogenous 11-*cis*-retinal (Fig. 5*C*, green lines; *SI Appendix*, *Supplementary Methods*). Incidentally, incubating unbleached, dark-adapted mouse rods with 11-*cis*-retinal did not have any obvious effect on dark noise (*SI Appendix*, Fig. S2), confirming previous reports of relatively negligible Opn in the absence of bleaching (28–31).

The cohort difference in values between pre- and postbleach dark-current means and variances measured as described can be analyzed to extract the amplitude and the frequency of the unitary responses (32, 33), as described as follows.

One WT-Opn Molecule Constitutively Produces ~1 Single-G_T*·PDE* Effect per Day. In the 5%-bleach experiment of Fig. 5 *B* and *C*, the changes in steady–dark-current mean and noise variance increased linearly ($R^2 = 0.95$ and $R^2 = 0.99$, respectively) with the number of WT-Opns produced by bleaching (*SI Appendix*, Table S2), consistent with a Poisson process underlying the occurrence of WT-Opn–associated electrical events. With this premise, the event amplitude is given by the postbleach dark current's variance/mean ratio (i.e., after subtracting unbleached dark values; *SI Appendix*, *Supplementary Methods*), taking into account the underlying unitary event's waveform determined from the

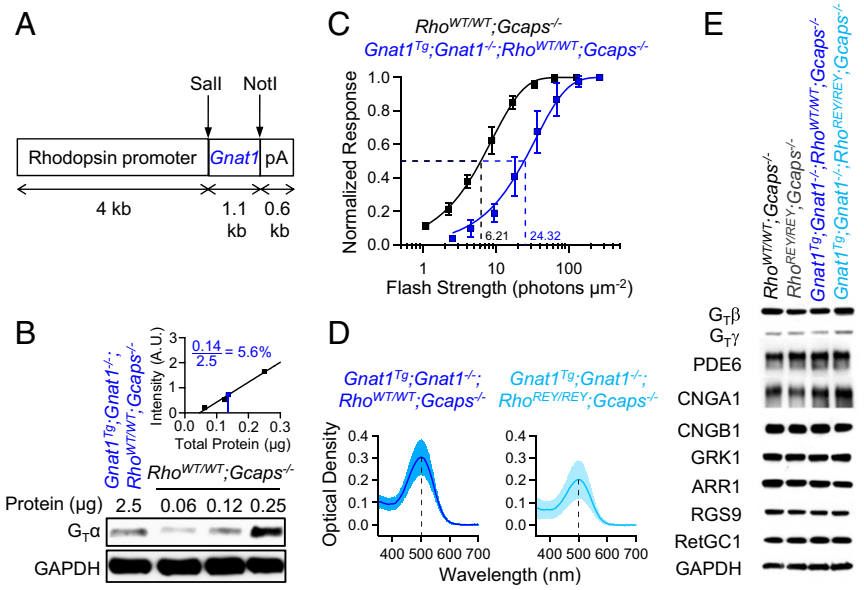

Fig. 4. Generation and characterization of *Gnat1*^{Tg};*Gnat1*$^{-/-}$ mice. (*A*) Construct design for the generation of *Gnat1*^{Tg} mice. (*B*) Western blot quantification of $G_T\alpha$ protein in *Gnat1*^{Tg};*Gnat1*$^{-/-}$;*Rho*$^{WT/WT}$;*Gcaps*$^{-/-}$ retinae. Dilution of *WT* protein extracts produced a calibration curve for comparison in band intensities with *Gnat1*^{Tg};*Gnat1*$^{-/-}$;*Rho*$^{WT/WT}$;*Gcaps*$^{-/-}$ (*SI Appendix, Supplementary Methods*). $G_T\alpha$ protein is expressed at ∼6% of *WT* in *Gnat1*^{Tg};*Gnat1*$^{-/-}$;*Rho*$^{WT/WT}$;*Gcaps*$^{-/-}$ retinae. Similar results were produced in several other experiments. (*C*) Intensity–response relations of *WT* (black, $n = 8$; reproduced from Fig. 2*C*) and *Gnat1*^{Tg};*Gnat1*$^{-/-}$;*Rho*$^{WT/WT}$;*Gcaps*$^{-/-}$ (blue, $n = 12$) rods. Fitting with a single saturating-exponential function gave half-saturating flash strengths (ρ) of 6.21 and 24.32 (equivalent 500-nm) photons·μm^{-2} for the two genotypes, respectively. Data points are means ± SD. (*D*) Absorption spectra of *Gnat1*^{Tg};*Gnat1*$^{-/-}$;*Rho*$^{WT/WT}$;*Gcaps*$^{-/-}$ (*Left*) and *Gnat1*^{Tg};*Gnat1*$^{-/-}$;*Rho*$^{REY/REY}$;*Gcaps*$^{-/-}$ (*Right*) rods measured by in situ microspectrophotometry (*SI Appendix, Supplementary Methods*) show a normal absorption maximum of rhodopsin (cf. Fig. 1*D*). The reason for the lower expression levels of rhodopsin in the latter line is unclear, but this does not affect the fluctuation analysis (mean ± SD; $n = 8$). (*E*) Western blots showing the expression levels of various phototransduction components in retinal extracts from the indicated genotypes. The data for *WT* and *REY* are reproduced here from Fig. 1*E* for comparison.

cohort-averaged difference power spectrum (Fig. 5*D* and *SI Appendix, Supplementary Methods*). The unitary-event frequency could then be calculated from the postbleach noise variance or the change in steady mean current (*SI Appendix, Supplementary Methods*). In this manner, we obtained a unitary-event amplitude (a') of 0.29 ± 0.10 pA and an event frequency of 15.5 ± 5.8 s^{-1} (mean ± SD; $n = 15$ cells). Corresponding experiments with 1% and 8% bleaches gave similar a' values and event waveforms, with event frequencies roughly in proportion to the number of Opns formed, as one might expect (Fig. 6 *A* and *B* and *SI Appendix*, Table S2).

To check whether the aforementioned Opn-associated events indeed represented single-G_T*·PDE* effects, we repeated the bleaching experiments with *Gnat1*^{Tg};*Gnat1*$^{-/-}$;*Rho*$^{WT/WT}$;*Gcaps*$^{-/-}$ mouse rods, which underexpressed $G_T\alpha$ drastically (as described earlier). Despite an event waveform with a moderately slower decay (Fig. 6*C* and *SI Appendix*, Table S2) —this being in parallel to the slower recovery of the unitary light response described earlier for this genotype (Fig. 3*C*, *Left*, *Inset*)—as well as a stronger bleach required to achieve a comparable postbleach noise (Fig. 6*D*), such $G_T\alpha$-underexpressing rods nonetheless gave a' values similar to those for rods with normal $G_T\alpha$ level (Fig. 6*E* and *SI Appendix*, Table S2). In short, each postbleach unitary event is indeed likely to be mediated by one G_T*·PDE*.

Unlike the roughly constant profile of the unitary Opn-associated effect, the single-photon response decreased progressively in amplitude with higher bleaches (Fig. 6*F* and legend and *SI Appendix*, Table S1B). Thus, bleaching appeared to reduce the number of G_T*s activated by a Rho*, probably in part as a result of a shorter Rho* lifetime (*SI Appendix*, Fig. S1 and legend).

In the plot of event rate against Opn content [Fig. 6*B*, *Right*, taking 6.5×10^7 rhodopsins per mouse rod (25)], the slope of the linear-regression line (Fig. 6*B*, *Right*, dashed line; constrained to go through the origin) gives a molecular rate constant for WT-Opn of 8.6×10^{-6} events·s^{-1}. In other words, each WT-Opn molecule in situ constitutively elicits an electrical response mediated by one G_T*·PDE* at a frequency of approximately once per 1.3 d at 37 °C. In comparison, an in situ rhodopsin molecule at 37 °C spontaneously and irreversibly isomerizes in ∼160 y on average (14, 25, 34). Therefore, 11-*cis*-retinal serves as an extremely effective negative agonist by reducing WT-Opn's constitutive activity rate by ∼4.5×10^4-fold, while simultaneously rendering rhodopsin photosensitive and giving a single-photon response more than an order of magnitude larger than the noise events from an Opn*. Thus, by being able to resolve the unitary-event amplitude triggered by an Opn*, we also succeeded in quantifying the "effective" temporal stability of Opn in situ (only "effective" because the Opn $\rightleftharpoons$ Opn* transitions could be more frequent, but only a fraction led to G_T*).

As the decay end-product of Rho*, Opn is reported to remain heterogeneously phosphorylated for many hours afterward, at least in the high-bleach condition of 50–70% bleach, with the subsequent dephosphorylation being accelerated by lactate or by lowering oxygen to 20% from the usual 95% during storage of bleached retinae by a mechanism not fully understood (35). Bleaching also induces arrestin/transducin translocations between the rod outer segment and inner segment (36, 37), although such translocations may have recovered during the long time period experienced in our experiments. At the low bleaching levels we used, there is no straightforward way to quantify, with single-cell precision, the various Opn phosphorylation states or the degrees of arrestin/transducin translocations for correlation with noise measurements. If these phenomena did persist in our postbleach measurements and affect Opn's constitutive activity, this, in principle, would not affect our derived single-G_T*·PDE* effect profile but would potentially affect the molecular rate of Opn's constitutive activity, such as if dephosphorylated Opn produces G_T*s more frequently. A most recent report appeared claiming that Opn triggers responses as large as the Rho*-triggered single-photon response in *Gcaps*$^{-/-}$ rods (38). It is unclear whether

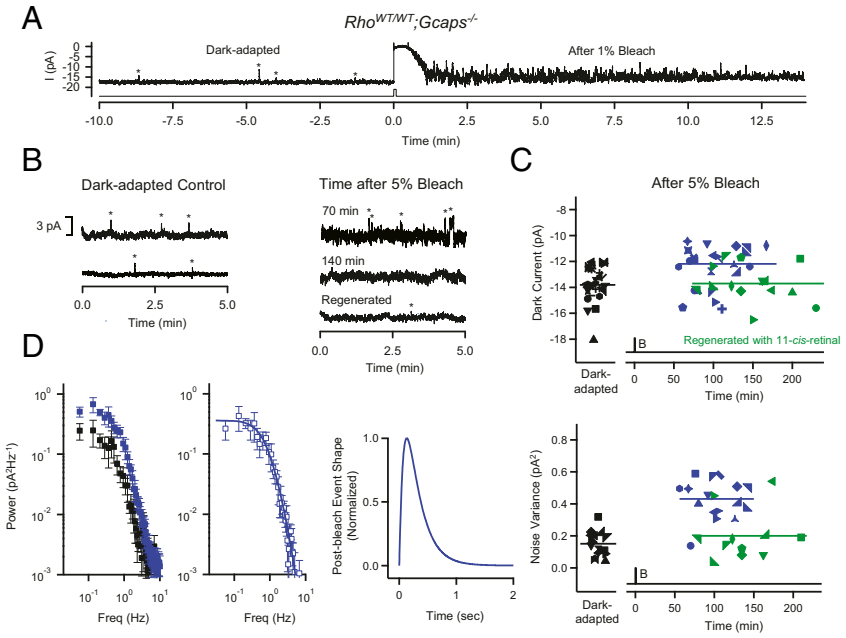

Fig. 5. Postbleach noise from Opn* in $Rho^{WT/WT};Gcaps^{-/-}$ rods. (*A*) Noise recording before and after bleaching ~1% of rhodopsin in a *WT* rod. (*B*, *Left*) Recordings from two different rods stored in darkness for >1 hr, showing steady current fluctuations (continuous noise) and occasional discrete events (marked with stars). (*Right*) Recordings from different rods after a 5% bleach and kept in darkness for 70 min, 140 min, or with similar bleach treatment, but subsequently incubated in 11-*cis*-retinal (*SI Appendix, Supplementary Methods*). (*C*) Steady–dark-current mean (*Top*) and continuous noise variance (*Bottom*) after a 5% bleach (blue), and after a 5% bleach followed by 11-*cis*-retinal incubation (green) for comparison with dark control rods (black). Each symbol represents a single cell. Solid lines show the cohort mean for each condition. From pairwise Student's *t* tests, we found a significant difference in noise variance between dark control and post-5% bleach rods ($P < 0.0001$) and between post-5% bleach rods and regenerated rods ($P < 0.0001$), but not between dark control rods and regenerated rods ($P = 0.26$). Correspondingly, there was a significant difference in dark-current mean between dark control and post-5% bleach rods ($0.0001 \leq P < 0.05$) and between post-5% bleach rods and regenerated rods ($0.0001 \leq P < 0.05$), but not between dark control rods and regenerated rods ($P = 0.82$). (*D*, *Left*) Cohort-averaged continuous-noise power spectra from dark control rods (black) and from post-5% bleach rods (blue). Each frequency point indicates cohort mean ± SEM ($n = 5$ rods). (*Middle* and *Right*) Difference spectrum and waveform of the unitary Opn* effect (transient peak normalized to unity) extracted from the difference spectrum by fitting with the spectrum of a convolution of two single-exponential declines (blue curve, $\tau_1 = 81 \pm 35$ msec, $\tau_2 = 231 \pm 25$ msec, $n = 5$ rods).

this difference in conclusion results from differences in specific experimental conditions or in data analysis (*SI Appendix*, *Supplementary Text II*).

Number of Single-G_T*·PDE* Effects Produced per WT-Rho* During the Single-Photon Response. Compared side by side, the single-G_T*·PDE* effect estimated from the REY-Rho experiments is smaller in amplitude but more prolonged temporally than that from the bleaching experiments (Fig. 7*A*, *Left*). These differences can be explained if, in the repeated-flash experiment, the consequential REY-Rho*s (i.e., those successful in eliciting electrical responses) had triggered their respective G_T*·PDE*s not all at the same time, but according to a temporal probability density function after the flash, hence stretching the G_T*-effect waveform in time after averaging over many trials. Indeed, the time integrals of the two single-G_T*·PDE* effect profiles (i.e., areas under the waveforms) were roughly equal, being 0.14 ± 0.03 pC ($n = 10$ cells) for REY-Rho* and 0.12 ± 0.04 pC ($n = 15$ cells) for WT-Opn* after a 5% bleach (Fig. 7*B*) or 0.12 ± 0.08 pC ($n = 37$ cells) for WT-Opn* when data from 1% and 8% bleaches are included. One potential factor contributing to the probability density function in *REY* rods is a long lifetime of REY-Rho*. However, spectroscopic measurements on heterologously expressed REY-Rho indicated that at least the postflash formation and decay of its meta-II state, which activates G_T, are not any slower than those of WT-Rho (*SI Appendix*, Fig. S3). In the in situ situation, on the other hand, there could still be a delay in the production of G_T* by REY-Rho*, in the phosphorylation of REY-Rho*, and in its subsequent binding by arrestin, all of which have been suggested to involve the ERY site or neighboring molecular surfaces (10, 39–42).

Interestingly, the time-integral values for the single-G_T*·PDE* effect we obtained from the other genotypes we used all lay within a fairly narrow range (Fig. 7*B*). Because we still do not fully understand the slightly varying kinetics in different conditions (e.g., slower decay in the $G_T\alpha$ underexpressor), we shall not pursue this feature here.

Dividing the time-integrated profile of the *WT* single-photon response (1.66 ± 0.52 pC, $n = 23$; Fig. 7*B*) by the corresponding mean value of the single-G_T*·PDE* effect (0.14 pC from REY-Rho* experiments and 0.12 pC from WT-Opn* experiments), both in $Gcaps^{-/-}$ background, yields an estimate of 12–14 G_T*·PDE* effects per WT-Rho*. We expect a similar value in the $Gcaps^{+/+}$ genotype because the GCAP proteins operate downstream of rhodopsin. This calculation assumes that single-G_T*·PDE* effects sum linearly during the WT-Rho* response. There is currently no clear evidence of any significant nonlinearity. For example, the single-photon–response amplitude from a WT-Rho* appears to decrease roughly in proportion to the number of G_T*-PDE*s produced when Rho*'s effective lifetime is shortened (17).

It is worth here to go a little further into the physical correlate of the single-G_T*·PDE* effect. A generally accepted picture today is that each Rho*-produced G_T* successfully finds and activates one of the two catalytic subunits (PDEα or PDEβ subunit) on the functionally symmetrical PDE dimeric complex (3, 43), giving rise to the measured "single-G_T*·PDE* effect," or half of the PDE-dimer activity (44, 45). As such, the total number of effective G_T*s produced by one Rho* should also be 12–14 as derived here earlier. In this picture, of course, two singly bound G_T*·PDE*s are functionally no different from one doubly bound G_T*·PDE*. Alternatively, however, the PDE-dimer

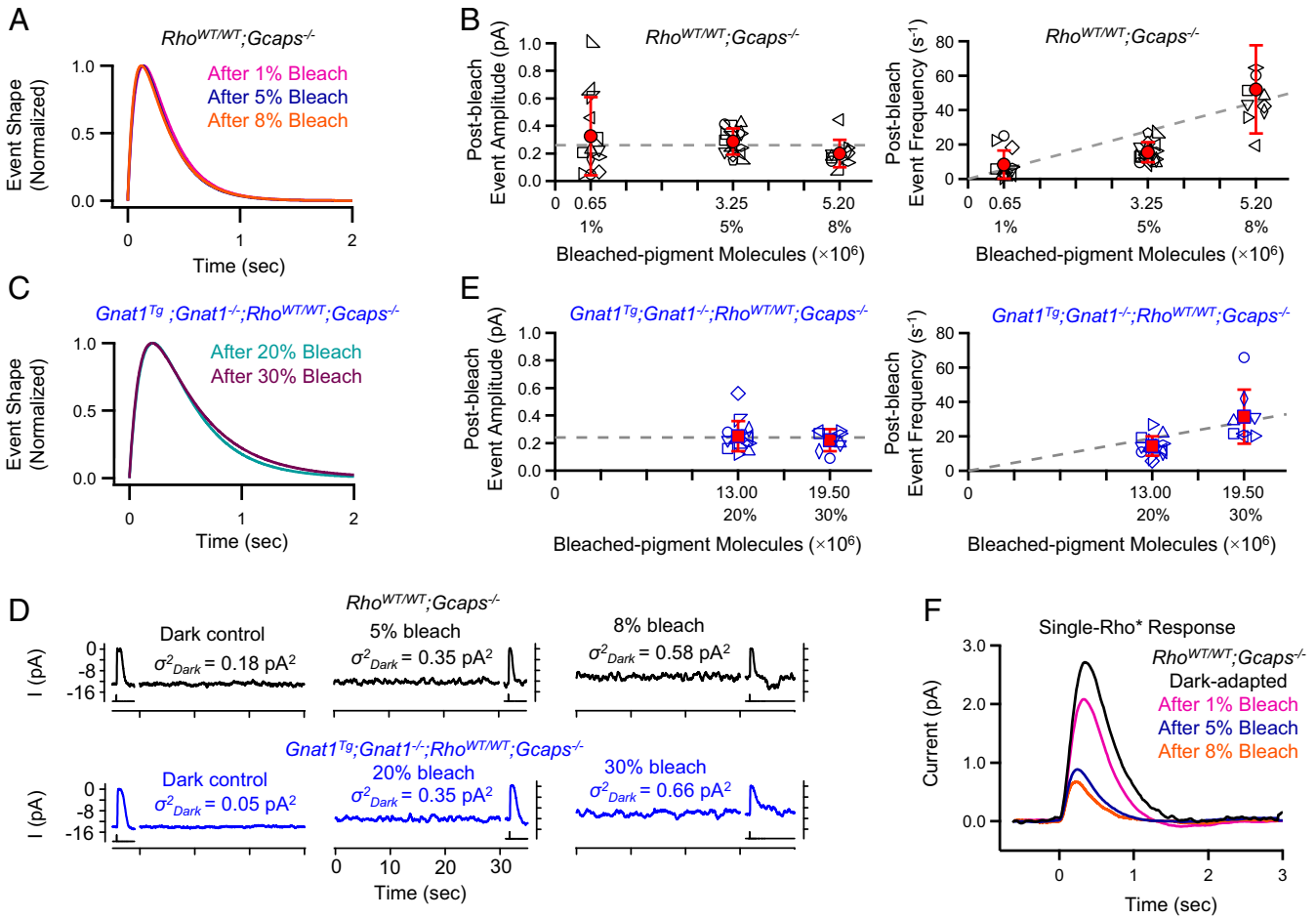

Fig. 6. Unitary G_T*·PDE* events underlying constitutive Opn*-triggered activity in $Rho^{WT/WT};Gcaps^{-/-}$ rods. (*A*) Waveform of unitary Opn* effects after a 1%, 5%, or 8% bleach (transient peak normalized to unity) extracted from difference spectra as in Fig. 5*D* (time constants in *SI Appendix*, Table S2). (*B*, *Left*) Unitary amplitudes of Opn-triggered events underlying postbleach noise after different bleaches of *WT* rods, derived from noise analysis (*SI Appendix*, *Supplementary Methods*). There was not a significant difference in amplitude across all bleaching conditions ($P = 0.27$, one-way ANOVA). Dashed line is the population mean amplitude from all bleach levels (each symbol represents a single cell). (*B*, *Right*) Cellular rate of events after different bleaches with percentage of total pigment content indicated below. Dashed line is a linear regression line passing through the origin ($R^2 = 0.8$) with slope giving a molecular rate constant of 8.6×10^{-6} events·s^{-1}·Opn^{-1}. (*C*) Waveform of unitary Opn* effects after a 20% or 30% bleach (transient peak normalized to unity) extracted from difference spectra as in Fig. 5*D*, but with the $Gnat1^{Tg};Gnat1^{-/-};Rho^{WT/WT};Gcaps^{-/-}$ line (time constants in *SI Appendix*, Table S2). (*D*, *Top*) Recordings from dark control (*Left*), 5%-bleached (*Middle*), and 8%-bleached (*Right*) rods from $Rho^{WT/WT};Gcaps^{-/-}$ mice. (*D*, *Bottom*) Similar recordings from dark control (*Left*), 20%-bleached (*Middle*), and 30%-bleached $Gnat1^{Tg};Gnat1^{-/-};Rho^{WT/WT};Gcaps^{-/-}$ rods with reduced $G_T\alpha$ expression. Zero-current axes are aligned to illustrate the approximate magnitude of the change in dark current after bleaching. (*E*) Same analysis as *B* but with $Gnat1^{Tg};Gnat1^{-/-};Rho^{WT/WT};Gcaps^{-/-}$ rods after a 20% or 30% bleach. (*Left*) Unitary amplitudes of Opn-triggered events were not significantly different from *WT* rods ($P = 0.34$, one-way ANOVA), and (*Right*) the event rate increased approximately in proportion to the amount of Opn formed ($R^2 = 0.8$, molecular rate constant = 1.5×10^{-6} s^{-1}·Opn^{-1}). (*F*) Averaged single-photon responses from WT-Rho* in dark-adapted *WT* rods as well as after a 1%, 5%, and 8% bleach.

has also been proposed to be functionally asymmetrical. One model posits that the singly bound G_T*·PDE* dimer has negligible activity, but reaches full dimeric activity when doubly bound by G_T* (46–48). Another posits the opposite scenario, with the singly bound G_T*·PDE* dimer already having literally full dimeric activity and the doubly bound G_T*·PDE* having negligible incremental activity (43). In either of these cases, the "single-G_T*·PDE* effect" we measured would actually correspond to the fully activated PDE-dimer species. Accordingly, the total number of bound G_T*s underlying the activated PDE activity could hypothetically be as much as two times of ∼12–14. Because these alternative models are rather tentative, we shall not go further into them here. In any case, regardless of the exact physical entity underlying the "single-G_T*·PDE* effect," our measurements suggest an effective gain of ∼12–14 at the receptor-to-effector step in phototransduction.

Discussion

Before the present work, the amplification factor at the Rho*-to-G_T* step in rod phototransduction and related parameters have been studied extensively, but no unanimous agreement had been reached. Early work (2) publicized the concept of a high amplification consisting of hundreds of G_T* per Rho*. Over the years, many other estimates have been suggested, including some much lower numbers more recently (9) (*SI Appendix*, *Supplementary Text I*), but, overall, they still range from teens to hundreds of G_T*s per Rho*. The reasons for such diverse estimates may come variably from nonnative preparations, uncertain temperature correction, differences in theoretical assumptions/parameters, or the downright uncertain nature of a monitored signal (*SI Appendix*, *Supplementary Text I*). Perhaps because of the lack of a definitive, unanimous agreement, the original notion of a very high gain has continued to take hold, and remains frequently quoted in textbooks and even generalized to other GPCR pathways (see the Introduction). Our measurements

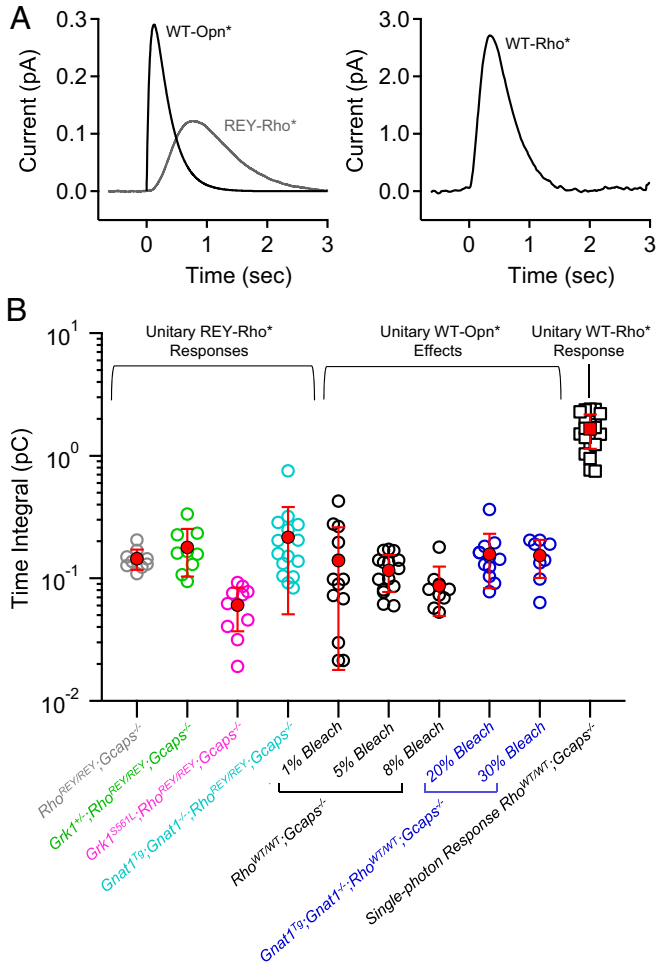

Fig. 7. Comparison of individual G_T*·PDE* effects with the unitary WT-Rho* response. (*A*, *Left*) Ensemble averages of single-G_T*·PDE* effect profiles produced by WT-Opn* (n = 15) after a 5% bleach and by REY-Rho* in *REY* rods (n = 10). (*A*, *Right*) Ensemble average of the unitary WT-Rho* response in dark-adapted *WT* rods (n = 23). All measurements were in the *Gcaps*$^{-/-}$ background for facilitating analysis of small responses. (*B*) Time-integrated profiles of single-G_T*·PDE* effects and the single-WT-Rho* response. Each open symbol represents a single cell. Closed symbols are means ± SD. The time-integrated single-G_T*·PDE* effects from all conditions were all within a range approximately an order of magnitude lower than that of the single-photon response from WT-Rho*. There was not a significant difference in values when comparing time-integrated profiles of single-G_T*·PDE* effects from REY-Rho* with those from WT-Opn (P = 0.21, Student's t test).

reported here based on two independent methods have converged on a unitary single-G_T*·PDE* effect that is only 1/10th to 1/20th of the single-photon response. This estimate is derived solely from direct measurements on intact rods and focuses on the effective signaling unit (i.e., single-G_T*·PDE* effect), which is much more relevant than merely the total number of G_T*s of uncertain consequence produced per Rho*. Hopefully, we have finally settled the longstanding dispute about the amplification in this step of phototransduction. Interestingly, in *Drosophila* phototransduction, which is a G protein/PLC-mediated pathway, the effective gain during the single-photon response was estimated to be ~5 $G_q\alpha$*·PLC* effector complexes based on a comparison of the WT unitary response with those of hypomorphs expressing low levels (<1%) of $G_q\alpha$ or PLC (49). Thus, receptor-to-effector gain in the most well-known phototransduction pathways may be more similar than previously thought.

Apart from phototransduction, little is known about the amplification at the GPCR*-to-G*/effector step in almost all other systems, which are very predominantly activated by ligands. The only ligand-triggered GPCR signaling pathway with related quantitative information available is vertebrate olfactory transduction. Surprisingly, the amplification factor in this case appears to be much less than 1 $G\alpha_{olf}$*·ACIII* per receptor–ligand binding event in native olfactory receptor neurons (50), where $G\alpha_{olf}$* is the active α-subunit of G_{olf} and ACIII* is an active adenylyl cyclase type III molecule mediating olfactory transduction. This low gain results at least in part from a brief dwell time of the odorant ligand on its receptor—perhaps no more than 1 ms or less at least for some receptor-odorant interactions (50)—vs. the relatively much longer Rho* lifetime. In preliminary work, one of the present authors (K.-W.Y.) has found such low gain even for cognate receptor–odorant interactions. Thus, a much lower gain than in rod phototransduction may be the norm in olfactory transduction.

The functional significance of this gain difference between phototransduction and olfactory transduction may be rationalized as follows. First, a low affinity between odorant and receptor in olfaction (which most likely explains the short active receptor lifetime) may be desirable by allowing some odorant receptors to recognize a wide variety of chemicals. Second, the overall amplification in the olfactory signaling circuit is drastically enhanced by a substantial axonal convergence; namely, on average, ~10^4 olfactory receptor neurons expressing the same odorant receptor species converge on the same glomerulus in the mouse olfactory bulb (51). In contrast, vision in an extremely dim environment demands not only exquisite sensitivity (down to single-photon detection) but also spatial acuity, but the latter would be severely degraded by a highly convergent visual neural circuitry. Third, unlike an odorant molecule, which, upon dissociation, can rebind to the same or another receptor, photons disappear instantly whether absorbed or not. Perhaps for these reasons, visual transduction requires a relatively high gain at the single-receptor–molecule level.

It is conceivable that ligand-driven signaling in general has a low GPCR-to-G protein/effector amplification because single-ligand–molecule detection or single-receptor–molecule signaling is not always essential (unless the availability of ligand is exceedingly low). A high gain may even be disadvantageous by causing rapid signal saturation and thus a low dynamic range. Furthermore, additional amplification downstream of the G protein is common by involving effector-enzyme or ion-channel activity. Finally, the overall sensitivity of a cell to stimulus can be substantially scaled up by increasing the receptor density on the plasma membrane. Thus, there are multiple ways to enhance sensitivity and signal amplification besides the G protein step. A number of early studies on isolated erythrocyte membranes and vesicle reconstitution systems have suggested that some (52–54) but not other (55) GPCRs could catalyze the activation of multiple G protein molecules per receptor molecule. However, these experiments did not provide definitive quantification because of their nonnative settings and ambiguities in what they exactly measured. In any case, it would be very useful to collect more information regarding the amplification question at the G protein level in other GPCR pathways and see how specific values are correlated with functions. For example, one question is whether the "mere" gain of ~12–14 in phototransduction is already at the high end for GPCR signaling.

Our work here has also provided biophysical information about the constitutive activity of WT-Opn. Psychophysical experiments demonstrated long ago that the human visual threshold does not increase linearly with the fraction of bleached pigment as would be expected from a simple loss of light-absorbing Rho, but much more steeply (56). The extradesensitizing effect of photobleaching was eventually found to come from Opn's constitutive ability to activate the phototransduction pathway, thus behaving as an "equivalent background light" (12). Until the present work, however, very little was known about the size of the associated electrical events and their frequency underlying this phenomenon. Given Opn*'s exceedingly weak activity, but

nonetheless acting through the same pathway as phototransduction, our speculation is therefore that the underlying unitary signal may be the same as the single-G_T*·PDE* effect. This speculation turns out to be correct. Furthermore, we found the frequency of these events to be, on average, approximately one event per day per Opn. Because we can only detect the unitary electrical events successfully triggered by Opn*, we do not yet know the molecular kinetics underlying Opn activation. In other words, it is unknown how frequently Opn actually transitions into the Opn* state, how much time it stays in this active state, and the probability that a collision event between Opn* and G_T will give a G_T*. This probability may or may not be the same as the probability of success for producing G_T* by Rho*.

What is clear is that, by comparing the spontaneous isomerization rate of rhodopsin to the constitutive activity of Opn quantified by us, 11-*cis*-retinal acts as an extremely potent negative agonist of Opn by reducing WT-Opn's effective constitutive activity rate by ~4.5×10^4-fold (*Results*), in addition to endowing Opn with photosensitivity. Opn's constitutive activity interferes with vision in dim light, given that even a 1% bleach introduces significant steady noise. On the contrary, Opn signaling also leads to bleaching adaptation, without which vision would be limited to a narrow range of light intensities. This Opn property is especially crucial for cone vision, which functions in bright light and is therefore invariably associated with the steady presence of Opn. On the negative side, however, Opn will also aggravate retinal diseases that lead to 11-*cis*-retinal deficiency, in that loss of chromophore not only reduces photon capture, but the resulting abundant Opn also generates noise, thereby degrading the signal-to-noise ratio even further.

Methods

Generation of *Rho$^{REY/REY}$* Knock-In Mice. All animal experiments were conducted according to protocols approved by the Institutional Animal Care and Use Committee at Johns Hopkins University. *Rho$^{REY/REY}$* mice were generated by using the CRISPR/Cas system. Briefly, the CRISPR Design Tool was used to select two 20-bp target sequences (5′-TTG AGC GCT ACG TGG TGG TC-3′ and 5′-CCG ATG AGC AAC TTC CGC TT-3′) close to the desired mutation site in the mouse rhodopsin gene. For each target sequence, cDNA oligos were synthesized, annealed, and cloned into the pX330 vector (Addgene) upstream of the transactivating CRISPR RNA sequence to give a chimeric single-guide RNA (sgRNA) sequence. The PCR-amplified product of this chimeric sequence was used as a template for in vitro transcription with the T7 Quick High Yield RNA synthesis kit (New England Biolabs). Each of the resulting sgRNAs was mixed with Cas9 mRNA (TriLink Biotechnologies) and a 166-bp synthesized oligo (5′-AGG TTA GAG CTG GAG GAC TGA CGG CTA CTA ACT GCC TTA CAG GTG AAA TCG CCC TGT GGT CCC TGG TGG TCC TGG CCA TTC GCG AGT ACG TGG TGG TCT GCA AGC CGA TGA GCA ACT TCC GCT TCG GGG AGA ATC ACG CCA TCA TGG GTG TGG TCT TCA CCT GGA T-3′; Integrated DNA Technologies) for homology-directed repair. The mixture for each sgRNA was injected separately into the pronuclei of *Gcaps$^{+/-}$* embryos at the transgenic core laboratory of Johns Hopkins University School of Medicine. Animals with the targeted mutation were identified by PCR on tail DNA and confirmed by sequencing. A set of three primers were used to genotype the rhodopsin allele: RhoWT forward, 5′-TGG TCC TGG CCA TTG AGC GC-3′; RhoREY forward, 5′-TGG TCC TGG CCA TTC GCG AG-3′; and Rho reverse, 5′-CCT GGA ACC AAT CCG AGG GC-3′. The primer pair of RhoWT forward and Rho reverse gave a 226-bp band for the WT allele, whereas the pair of RhoREY forward and Rho reverse gave a band of the same size for the mutant allele. Genomic PCR did not reveal any unintended mutations at off-target sites predicted by the CRISPR Design Tool. To reduce any potential off-target effect, the line has further been crossed at least two times to *Gcaps$^{-/-}$* mice.

Suction-Pipette Recording. Mice 1–3 mo of age were used for experiments. Under dim red light, an eye was removed from an acutely euthanized mouse, with the retina isolated under infrared illumination into Locke's solution [112.5 mM NaCl, 3.6 mM KCl, 2.4 mM $MgCl_2$, 1.2 mM $CaCl_2$, 3 mM Na_2-succinate, 0.5 mM Na-glutamate, 0.02 mM EDTA, 10 mM glucose, 0.1% MEM vitamins (M6895; Sigma-Aldrich), 0.1% MEM amino acid supplement (M5550; Sigma-Aldrich), 10 mM Hepes, pH 7.4, and 20 mM $NaHCO_3$]. The retina was divided into three pieces, one used immediately for recording and the others stored in Locke's solution bubbled with 95% O_2/5% CO_2 at room temperature until use over 6 h or less.

When needed, a piece of retina was chopped into small fragments on a Sylgard plate (24236-10; Electron Microscopy Sciences) with a razorblade in the presence of DNase I (~20 U/mL). The tissues were then transferred to a recording chamber perfused with Locke's solution at 37.5 ± 0.5 °C. Temperature was monitored by a thermistor situated adjacent to the recorded cell. Single-cell recordings were made under IR light by drawing the outer segment of a rod projecting from a retinal fragment into a tight-fitting glass pipette containing 140 mM NaCl, 3.6 mM KCl, 2.4 mM $MgCl_2$, 1.2 mM $CaCl_2$, 0.02 mM EDTA, 10 mM glucose, and 3 mM Hepes, pH 7.4.

Light stimulation was usually 10–30-ms monochromatic (for most experiments) or white flashes (for highly insensitive rods, e.g., *Rho$^{REY/REY}$;Gcaps$^{-/-}$* rods); in the latter case, the intensities equivalent to 500-nm light were calculated by matching the amplitudes of small responses elicited by white light against those by 500-nm light. Signals were sampled at 2 kHz through an Axopatch 200B amplifier and low-pass filtered through two separate channels at 1 kHz and 20 Hz (RC filter, model 3343; Krohn-Hite). The 1-kHz and 20-Hz channels were compared in order to measure the time delay (~58–63 ms) caused by 20-Hz filtering. This delay was corrected. Unless otherwise specified, recording traces presented in figures are 20-Hz filtered.

Bleaching and Retina-Storage Procedure. For bleaching experiments, a retina was peeled away from the RPE while immersed in prebubbled (95% O_2/5% CO_2) Locke's solution, with the addition of lipid-free BSA (1 mg/mL, A6003; Sigma-Aldrich) to facilitate clearance of all-*trans*-retinoids after bleaching (22). Under infrared illumination, the retina was flat-mounted in solution on a piece of black filter paper (HABP02500; Merck Millipore) with photoreceptors facing upward. A Petri dish containing the flat-mounted retina was placed on a platform centered vertically under a LED light source (λ_{max} = 470 nm) equipped with an aspherical collimating lens (M470L2; Thor Labs) and a 10-nm band-pass filter centered at 480 nm. This wavelength was used simply because the lighting fixture was available in the laboratory. The bleaching calculations (*SI Appendix, Supplementary Methods*) took into account the sensitivity of rhodopsin to 480-nm relative to 500-nm light. Light intensity was calibrated before each experiment. The flat-mounted retina was exposed to a light step calculated to bleach a targeted number of rhodopsin molecules (*SI Appendix, Supplementary Methods*). Immediately following bleaching, ~1–2 mm^2 of tissue was cut from the central retina to ensure vertical orientation for approximately uniform bleaching, with light traveling down the long axis of the outer segment.

Bleached retinal tissue was transferred to a storage chamber consisting of a silane-coated glass slide at the bottom of a plastic-walled chamber. A gentle stream of O_2/CO_2 was blown across the surface of the solution, not far (~4 mm) from the tissue sitting at the bottom of the chamber. The volume of storage solution was kept approximately constant (changing by <5% over 30 min) with a syringe of distilled water dripping through a 33-gauge needle at a rate approximately equal to the evaporation rate (verified before each experiment). This method allowed storage with good O_2/CO_2 supply but without foaming of the BSA–Locke's solution. After 30 min of storage, the tissue was finely chopped in Locke's solution without BSA on a Sylgard plate and transferred to the recording chamber. Photoisomerized rhodopsin transitions through several intermediate states [metarhodopsin (meta)-I, -II, and -III] before releasing all-*trans*-retinal to become Opn. In mouse rods, meta-II decays with a biexponential time course (time constants of ~4 and 16 min at 37 °C) with ~5% of meta-II signal remaining at 30 min after light onset (22). Meta-III decay is slower, with >10% meta-III signal remaining at 30 min after light onset (22, 57). Although meta-III cannot activate G_T, it can occasionally convert back to meta-II (58). To record exclusively from noise originating from Opn molecules, bleached rods were recorded 1–3 h after bleaching (allowing sufficient time for photointermediates to decay to Opn).

All additional experimental details are provided in *SI Appendix, Supplementary Methods*.

ACKNOWLEDGMENTS. We thank Drs. Ching-Kang Jason Chen (Baylor College of Medicine) and Janis Lem (Tufts University) for the *Grk1^{5561L}* and *Gnat1$^{-/-}$* mouse lines, respectively; Drs. Robert S. Molday (University of British Columbia), Alexander M. Dizhoor (Salus University), Ching-Kang Jason Chen (Baylor College of Medicine), and Theodore G. Wensel (Baylor College of Medicine) for antibodies; and Drs. Marie E. Burns and Edward N. Pugh, Jr. (University of California, Davis), Trevor D. Lamb (Australian National University), Jeremy Nathans and Randall Reed (Johns Hopkins University), David Julius and Nicholas Bellono (University of California, San Francisco), Donggen Luo (Peking University), and members of the K.-W.Y. laboratory for discussions. This work was supported by National Institutes of Health Grants EY006837 (to K.-W.Y.), EY001157 (to M.C.C.), and EY012155 (to J.C.); the António Champalimaud Vision Award, Portugal (to K.-W.Y.); a Howard Hughes Medical Institute International Predoctoral Fellowship (to W.W.S.Y.); and Visual Science Training Program Fellowship EY007143 from the National Eye Institute (to D.S.).

1. Baylor DA, Lamb TD, Yau K-W (1979) Responses of retinal rods to single photons. *J Physiol* 288:613–634.
2. Vuong TM, Chabre M, Stryer L (1984) Millisecond activation of transducin in the cyclic nucleotide cascade of vision. *Nature* 311:659–661.
3. Leskov IB, et al. (2000) The gain of rod phototransduction: Reconciliation of biochemical and electrophysiological measurements. *Neuron* 27:525–537.
4. Alberts B, et al. (2015) Second messengers and enzymatic cascades amplify signals. *Molecular Biology of the Cell* (Garland Science, New York), 6th Ed, p 869.
5. Kandel ER, Schwartz JH, Jessel TM, Siegelbaum SA, Hudspeth AJ (2012) Low-level visual processing: The retina. *Principles of Neural Science* (McGraw-Hill Education, New York), 5th Ed, p 583.
6. Nicholls JG, Martin AR, Wallace BG (2011) Transduction and transmission in the retina. *From Neuron to Brain* (Sinauer, Sunderland, MA), 5th Ed, p 417.
7. Purves D, et al. (2011) Amplification in signal transduction pathways. *Neuroscience* (Sinauer, Sunderland, MA), 5th Ed, p 143.
8. Lesk A (2016) G proteins and G-protein-coupled receptors. *Introduction to Protein Science: Architecture, Function, and Genomics* (Oxford Univ Press, New York), 3rd Ed, p 84.
9. Arshavsky VY, Burns ME (2014) Current understanding of signal amplification in phototransduction. *Cell Logist* 4:e29390.
10. Franke RR, König B, Sakmar TP, Khorana HG, Hofmann KP (1990) Rhodopsin mutants that bind but fail to activate transducin. *Science* 250:123–125.
11. Sakmar TP, Franke RR, Khorana HG (1989) Glutamic acid-113 serves as the retinylidene Schiff base counterion in bovine rhodopsin. *Proc Natl Acad Sci USA* 86: 8309–8313.
12. Cornwall MC, Fain GL (1994) Bleached pigment activates transduction in isolated rods of the salamander retina. *J Physiol* 480:261–279.
13. Mendez A, et al. (2001) Role of guanylate cyclase-activating proteins (GCAPs) in setting the flash sensitivity of rod photoreceptors. *Proc Natl Acad Sci USA* 98: 9948–9953.
14. Fu Y, Kefalov V, Luo D-G, Xue T, Yau K-W (2008) Quantal noise from human red cone pigment. *Nat Neurosci* 11:565–571.
15. Okawa H, et al. (2010) Optimal processing of photoreceptor signals is required to maximize behavioural sensitivity. *J Physiol* 588:1947–1960.
16. Chen C-K, et al. (2012) Modulation of mouse rod response decay by rhodopsin kinase and recoverin. *J Neurosci* 32:15998–16006.
17. Gross OP, Pugh EN, Jr, Burns ME (2012) Calcium feedback to cGMP synthesis strongly attenuates single-photon responses driven by long rhodopsin lifetimes. *Neuron* 76: 370–382.
18. Chen C-K, et al. (1999) Abnormal photoresponses and light-induced apoptosis in rods lacking rhodopsin kinase. *Proc Natl Acad Sci USA* 96:3718–3722.
19. Calvert PD, et al. (2000) Phototransduction in transgenic mice after targeted deletion of the rod transducin alpha -subunit. *Proc Natl Acad Sci USA* 97:13913–13918.
20. Pugh EN, Jr, Lamb TD (1993) Amplification and kinetics of the activation steps in phototransduction. *Biochim Biophys Acta* 1141:111–149.
21. Melia TJ, Jr, Cowan CW, Angleson JK, Wensel TG (1997) A comparison of the efficiency of G protein activation by ligand-free and light-activated forms of rhodopsin. *Biophys J* 73:3182–3191.
22. Nymark S, Frederiksen R, Woodruff ML, Cornwall MC, Fain GL (2012) Bleaching of mouse rods: Microspectrophotometry and suction-electrode recording. *J Physiol* 590: 2353–2364.
23. Baylor DA, Matthews G, Yau KW (1980) Two components of electrical dark noise in toad retinal rod outer segments. *J Physiol* 309:591–621.
24. Rieke F, Baylor DA (1996) Molecular origin of continuous dark noise in rod photoreceptors. *Biophys J* 71:2553–2572.
25. Luo D-G, Yue WWS, Ala-Laurila P, Yau K-W (2011) Activation of visual pigments by light and heat. *Science* 332:1307–1312.
26. Lamb TD (1980) Spontaneous quantal events induced in toad rods by pigment bleaching. *Nature* 287:349–351.
27. Leibrock CS, Lamb TD (1997) Effect of hydroxylamine on photon-like events during dark adaptation in toad rod photoreceptors. *J Physiol* 501:97–109.
28. Kefalov VJ, et al. (2005) Breaking the covalent bond–A pigment property that contributes to desensitization in cones. *Neuron* 46:879–890.
29. Luo D-G, Yau K-W (2005) Rod sensitivity of neonatal mouse and rat. *J Gen Physiol* 126: 263–269.
30. Xiong W-H, Yau K-W (2002) Rod sensitivity during Xenopus development. *J Gen Physiol* 120:817–827.
31. Tian H, Sakmar TP, Huber T (2017) Measurement of slow spontaneous release of 11-cis-retinal from rhodopsin. *Biophys J* 112:153–161.
32. Rice SO (1944) Mathematical analysis of random noise. *Bell Syst Tech J* 23:282–332.
33. Katz B, Miledi R (1972) The statistical nature of the acetycholine potential and its molecular components. *J Physiol* 224:665–699.
34. Burns ME, Mendez A, Chen J, Baylor DA (2002) Dynamics of cyclic GMP synthesis in retinal rods. *Neuron* 36:81–91.
35. Berry J, et al. (2016) Effect of rhodopsin phosphorylation on dark adaptation in mouse rods. *J Neurosci* 36:6973–6987.
36. Strissel KJ, Sokolov M, Trieu LH, Arshavsky VY (2006) Arrestin translocation is induced at a critical threshold of visual signaling and is superstoichiometric to bleached rhodopsin. *J Neurosci* 26:1146–1153.
37. Sokolov M, et al. (2002) Massive light-driven translocation of transducin between the two major compartments of rod cells: A novel mechanism of light adaptation. *Neuron* 34:95–106.
38. Sato S, Jastrzebska B, Engel A, Palczewski K, Kefalov VJ (2018) Apo-opsin exists in equilibrium between a predominant inactive and a rare highly active state. *J Neurosci* 39:212–223.
39. Jones Brunette AM, Sinha A, David L, Farrens DL (2016) Evidence that the rhodopsin kinase (GRK1) N-terminus and the transducin Gα C-terminus interact with the same "hydrophobic patch" on rhodopsin TM5. *Biochemistry* 55:3123–3135.
40. Kang Y, et al. (2015) Crystal structure of rhodopsin bound to arrestin by femtosecond X-ray laser. *Nature* 523:561–567.
41. Palczewski K, Buczyłko J, Kaplan MW, Polans AS, Crabb JW (1991) Mechanism of rhodopsin kinase activation. *J Biol Chem* 266:12949–12955.
42. Szczepek M, et al. (2014) Crystal structure of a common GPCR-binding interface for G protein and arrestin. *Nat Commun* 5:4801.
43. Melia TJ, Malinski JA, He F, Wensel TG (2000) Enhancement of phototransduction protein interactions by lipid surfaces. *J Biol Chem* 275:3535–3542.
44. Wensel TG, Stryer L (1990) Activation mechanism of retinal rod cyclic GMP phosphodiesterase probed by fluorescein-labeled inhibitory subunit. *Biochemistry* 29: 2155–2161.
45. Muradov H, Boyd KK, Artemyev NO (2010) Rod phosphodiesterase-6 PDE6A and PDE6B subunits are enzymatically equivalent. *J Biol Chem* 285:39828–39834.
46. Qureshi BM, et al. (2018) It takes two transducins to activate the cGMP-phosphodiesterase 6 in retinal rods. *Open Biol* 8:180075.
47. Bennett N, Clerc A (1989) Activation of cGMP phosphodiesterase in retinal rods: Mechanism of interaction with the GTP-binding protein (transducin). *Biochemistry* 28: 7418–7424.
48. Lamb TD, Heck M, Kraft TW (2018) Implications of dimeric activation of PDE6 for rod phototransduction. *Open Biol* 8:180076.
49. Hardie RC, et al. (2002) Molecular basis of amplification in Drosophila phototransduction: Roles for G protein, phospholipase C, and diacylglycerol kinase. *Neuron* 36:689–701.
50. Bhandawat V, Reisert J, Yau K-W (2005) Elementary response of olfactory receptor neurons to odorants. *Science* 308:1931–1934.
51. Su CY, Menuz K, Carlson JR (2009) Olfactory perception: Receptors, cells, and circuits. *Cell* 139:45–59.
52. Tolkovsky AM, Levitzki A (1978) Mode of coupling between the β-adrenergic receptor and adenylate cyclase in turkey erythrocytes. *Biochemistry* 17:3795.
53. Tolkovsky AM, Braun S, Levitzki A (1982) Kinetics of interaction between beta-receptors, GTP protein, and the catalytic unit of turkey erythrocyte adenylate cyclase. *Proc Natl Acad Sci USA* 79:213–217.
54. Pedersen SE, Ross EM (1982) Functional reconstitution of beta-adrenergic receptors and the stimulatory GTP-binding protein of adenylate cyclase. *Proc Natl Acad Sci USA* 79:7228–7232.
55. Senogles SE, et al. (1987) The D2-dopamine receptor of anterior pituitary is functionally associated with a pertussis toxin-sensitive guanine nucleotide binding protein. *J Biol Chem* 262:4860–4867.
56. Rushton WA (1965) Visual adaptation. *Proc R Soc Lond B Biol Sci* 162:20–46.
57. Frederiksen R, et al. (2016) Rhodopsin kinase and arrestin binding control the decay of photoactivated rhodopsin and dark adaptation of mouse rods. *J Gen Physiol* 148: 1–11.
58. Chabre M, Breton J (1979) The orientation of the chromophore of vertebrate rhodopsin in the "meta" intermediate states and the reversibility of the meta II-meta III transition. *Vision Res* 19:1005–1018.